Zeolites

3D Raman Spectroscopy of Large Zeolite ZSM-5 Crystals

Özgün Attila,[a] Helen E. King,[b] Florian Meirer,[a] and Bert M. Weckhuysen*[a]

Abstract: Hydrothermal treatment is a common method used to modify the physicochemical properties of zeolite-based catalyst materials. It alters the number and type of acid sites through dealumination and increases molecular diffusion by mesopore formation. Steaming also reduces the structural integrity of zeolite frameworks. In this study, Raman microscopy has been used to map large zeolite ZSM-5 crystals before and after steaming. 3D elemental maps of T–O (T: Al or Si) sites of the zeolite were obtained. The Raman active vibrational bands were determined, which are indicative of (non-) framework Al, as well as of structural integrity. Zeolite steaming caused the introduction of additional heterogeneities within the zeolite framework. Al migration and the formation of extra-framework Al species were observed. The described experiments demonstrate the capability of 3D Raman spectroscopy as a valuable tool to obtain information on the spatial distributions of framework elements as well as defects within a zeolite-based material.

Introduction

The catalytic properties of zeolites are strongly determined by their Brønsted acidity, which is governed by the Si/Al ratio of the zeolite framework. Additionally, the spatial distribution of framework and extra-framework Al affects the overall reactivity of zeolites.[1–3] Hydrothermal treatment (i.e., steaming) causes pore enlargement by modifying the zeolite microporosity, which enhances the diffusion properties of the zeolite framework through dealumination. Upon steaming, framework Al species are removed forming non-framework Al sites.[4] Therefore, steaming alters the overall activity of zeolites.[5–14] A fine balance is required between the number of Brønsted acid sites (i.e., the amount of active sites) and the mesopore volume formed through steaming (i.e., improving the accessibility towards the active sites).

It is fair to state that vibrational spectroscopies are (one of) the major characterization tools utilized in zeolite science and technology as they can provide structural and bond information about the zeolite frameworks.[15,16] In particular, infrared (IR) spectroscopy has been one of the most common spectroscopic methods used to study the structure and reactivity of zeolite-based materials, often in combination with probe molecules, such as pyridine, ammonia, CO, and NO. In comparison to IR spectroscopy, Raman spectroscopy is rather under-utilized in zeolite science, mainly because of the difficulty of obtaining Raman spectra with reasonable signal-to-noise (S/N) ratio. However, the principle of confocality that is lacking in IR microscopy, makes Raman microscopy a useful tool for zeolite characterization.[16,17] The major difficulty of measuring Raman spectra of zeolites is attributed to the often-encountered broad fluorescence, which is an intrinsic property of zeolites.[18] Moreover, the presence of small amounts of organic molecules (mainly coming from template molecules used for the synthesis of zeolites) can also overshadow the characteristic (weak) Raman bands of the zeotype frameworks. This is because the spectrum of these organic molecules is massively enhanced when the laser frequency matches with the frequency of their electronic transitions; a process which is known as the resonance Raman effect.[19] High-temperature treatments under an oxidative atmosphere are reported to resolve the issue of organic impurities, as it is considered that these conditions are able to remove the hydrocarbon species responsible for fluorescence.[20]

The problem of broad fluorescence could be (partially) solved by using lasers of appropriate wavelength with respect to the type of materials researched.[16] Especially, UV lasers have helped to overcome the fluorescence problem in Raman spectroscopy of zeolites. Some active groups in this field of research include those of Li,[19] Dutta,[21] and Stair,[22] as well as of Lamberti, Zecchina and Bordiga[23] and we refer here to some of their seminal papers for further information. For example, it has been possible to probe the dealumination extent within the MFI framework using UV-Raman spectroscopy.[24] Similarly,

[a] Dr. Ö. Attila, Dr. F. Meirer, Prof. Dr. B. M. Weckhuysen
Inorganic Chemistry and Catalysis, Debye Institute for Nanomaterials Science
Utrecht University, Universiteitsweg 99
3584 CG Utrecht (The Netherlands)
E-mail: b.m.weckhuysen@uu.nl

[b] Dr. H. E. King
Department of Earth Sciences, Faculty of Geosciences
Utrecht University
Princetonlaan 8a, 3584 CB Utrecht (The Netherlands)

Supporting information and the ORCID identification number(s) for the author(s) of this article can be found under: https://doi.org/10.1002/chem.201805664.

Table 1. Literature survey of the Raman band assignments of zeolite ZSM-5.

Band position [cm^{-1}]	Vibrational mode assignments[a]	Ref.	Band position [cm^{-1}]	Vibrational mode assignments[a]	Ref.
294	δ (T-O-T) of 6MR	[32]	617	D4R	[33]
360	δ (D6R)	[15]	673	δ (Si-O-Al)	[34]
380	ν_s (T-O-T)	[21]	723	ν_s (T–O)	[35]
408	δ (O-T-O)	[36]	745	ν (Si-O-Al)	[24]
438	ν (Si-O-Si)	[37]	800	ν_s (Si-O-Si)	[38]
454	δ (O-Si-O(Al))	[39]	814	$\nu_{t,as}$ (Al–O)	[36]
470	δ (Si–O)	[40]	832	(Al^6–O)	[41]
548	D5R	[42]	890	δ (O-Si-H)	[38]
590	ν_s (Al-O-Si)	[29]	901	ν_m (D6R)	[36]
598	ν (Al-O-Si)	[21]	967	δ_m, ν_m (T–O)	[43]

[a] Notation for the various motions of atoms within the normal modes is defined as follows: ν, stretching; δ, bending; s, symmetric; as, asymmetric. #MR stands for the # membered ring vibration and D#R stands for the # membered double ring vibration.

temperature-dependent coke formation under hydrocarbon conversion process conditions in zeolites ZSM-5 and USY was also studied with Raman spectroscopy using a UV laser.[19]

The first assignments of vibrational bands of zeolites, however, were proposed by Flanigen and co-workers.[25] They based their assignments on a series of systematic IR investigations of silica, as well as non-zeolitic (silicate) minerals.[26] Over time, researchers categorized the variety of zeolite framework topologies and composition of bulk zeolite materials using vibrational spectroscopies.[15,19,23–25,27–30] The most intense Raman bands of zeolites are located between 300–600 cm^{-1}.[15] The bands in this spectral region are highly structure-sensitive, which means the occurrence of differently sized building units in the zeolite structure corresponds to different frequencies.[31]

As zeolites are generally constructed from TO_4 tetrahedra (T: tetrahedral atoms, such as Al, Si, P…), the most intense band in this spectral region is assigned to the vibration of an oxygen atom in a plane perpendicular to the T-O-T bonds.[1,15] It was shown that for zeolites containing only even-membered rings (MR) (i.e., 4MR, 6MR, 8MR.) this band is found at 500 cm^{-1}. Examples include CHA and FAU. In contrast, the presence of a 5MR lowers the main frequency of the band to 390–460 cm^{-1}. For instance, FER has an intense Raman band at 430 cm^{-1}, whereas MFI has this Raman band at 380 cm^{-1}.[21] Similarly, vibrational bands at 500–650 cm^{-1} and 300–420 cm^{-1} are due to external linkage vibrations, namely vibrations of double four-membered rings (D4R), double five-membered rings (D5R), or double six-membered rings (D6R), and pore opening vibrations, respectively.[32] The other dominant bands are reported to occur in the ranges 650–790 and 950–1250 cm^{-1}, which are tentatively assigned to the asymmetrical stretching mode of (O-T-O) and to the symmetrical stretching mode (O-T-O) of the TO_4 tetrahedra, respectively. Further band assignments for zeolite ZSM-5, as reported in various studies, are listed in Table 1. However, some of the Raman vibrational modes of zeolites are not clearly assigned due to the very similar physicochemical properties of Al and Si atoms, which are difficult to differentiate by vibrational spectroscopies. Therefore, some of the vibrations in the literature are stated as T–O where T refers to Al or Si atoms; they can be considered as tentative.

Here, we have studied the effect of steaming on the integrity of the structure of large zeolite ZSM-5 crystals with Raman microscopy. It is known from previous studies that the large zeolite ZSM-5 crystals used in this study (and synthesized using a TPA^+ template) have Al enrichment on the crystal edges and the outer surface.[44–48] In this work, parent (non-steamed) zeolite ZSM-5 crystals (further denoted as P-ZSM-5) are compared with two sets of steamed ZSM-5 crystals that are either mildly treated at 500 °C (further denoted as MT-ZSM-5) or severely treated crystals at 700 °C (further denoted as ST-ZSM-5). Previous studies with scanning electron microscopy (SEM) and atomic force microscopy (AFM) have demonstrated that there is no significant change in the overall morphology of the zeolite ZSM-5 crystal upon steaming under the above-written conditions.[11] It was also demonstrated that the central regions of the crystal do change their surface topography at the nanometer scale after steaming, whereas the tip regions show minimal alteration. These findings are summarized in section S1 (Figure S1) of the Supporting Information, whereas further details on these large zeolite ZSM-5 crystals can be found in the literature.[49–54]

By using the confocality of Raman microscopy, it becomes possible to map the spatial heterogeneities within the zeolite ZSM-5 crystals in 3D that are introduced by steaming. Furthermore, through a detailed comparison of the Raman spectra collected, we collected a set of fingerprint spectra along with plausible assignments of Raman bands related to framework and extra-framework Al, as well as defect sites, which could serve as inspiration for theoreticians to further refine the assignments of vibrational modes of zeolite-based materials.

Results and Discussion

Figure 1 shows the averaged 3D Raman spectra of the zeolite P-ZSM-5, MT-ZSM-5, and ST-ZSM-5 crystals in the region of 250–1000 cm^{-1}. The first striking difference in the Raman spectra of the three distinct zeolite ZSM-5 crystals is the variety of spectral intensity of the measurements. The intensity of the Raman scattered radiation, *I*, for a sample can be simply expressed using Equation (1):[55]

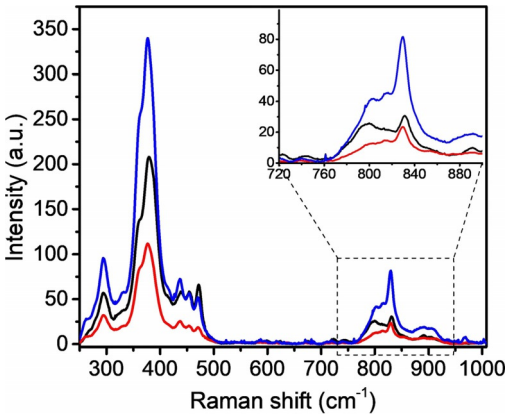

Figure 1. Averaged Raman spectra of the zeolite P-ZSM-5 (black), MT-ZSM-5 (red), and ST-ZSM-5 (blue) crystals. The spectral integration time was 7 s. The inset highlights the 720–900 cm^{-1} spectral region.

$$I \propto \nu^4 I_o N \left(\frac{\partial \alpha}{\partial Q}\right)^2 \quad (1)$$

where:

ν = Frequency of the exciting laser
I_o = Incident laser intensity
N = Number of scattering molecules
α = Polarizability of the molecules
Q = Vibrational amplitude

The term $\left(\frac{\partial \alpha}{\partial Q}\right)^2$ describes the change in polarizability caused by molecular vibrations. For a vibration to be Raman active it must cause a change in the polarizability. As the term is squared it becomes greater than zero. Considering a constant laser intensity and a fixed measurement geometry, the Raman band intensities are directly related to the number of scattering molecules, *N*. The number *N* depends on the analyte concentration and the illuminated volume. Nano- and micro-scale irregularities and physical defects are known to be present in zeolite crystals. So, at a given point, the focal volume may vary due to such defect sites. Furthermore, the Raman signals generated from a specific volume is expected to be different than the signal read by the spectrometer due to scattering effects, which is also dependent on the sample geometry and physical defects in the analyte volume.

In order to obtain accurate and quantitative spectral intensity, a normalization procedure was necessary to correct for overall intensity variations. Amongst the many normalization methods possible, we have used the method of "normalization with respect to maximum intensity".[56] The most prominent band detected in the spectrum of the parent zeolite ZSM-5 crystal was the O atom vibration within the T-O-T bond plane at 380 cm^{-1}.This band also remained the most intense Raman band in spectra for zeolite crystals that have been steamed. Therefore, we used the intensity of this Raman band as the denominator to normalize the spectra. In this way, the comparison of the relative spectral differences between the averaged Raman spectra of the pre- and post-steamed zeolite ZSM-5 crystals can be performed with greater accuracy. The result of the normalization is shown in Figure 2. The steaming procedure clearly produced spectral differences in the region of 400–500 cm^{-1} (indicated by the yellow area in Figure 2) in comparison to the parent ZSM-5 crystal. All the prominent

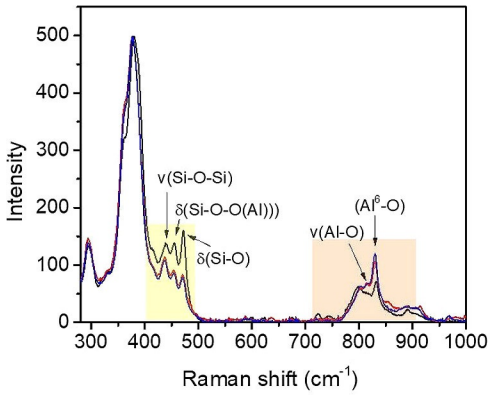

Figure 2. Normalized and averaged Raman spectra of zeolite P-ZSM-5 (black), MT-ZSM-5 (red) and ST-ZSM-5 (blue) crystals with indicated Raman band assignments, as summarized in Table 1.

bands in this region, that is, ν(Si-O-Si)[37] at 438 cm^{-1}, δ (O-Si-O(Al))[39] at 454 cm^{-1}, and δ (Si–O)[40] at 470 cm^{-1} were observed to decrease in intensity. The ν(Si-O-Si) band became the most intense of the three peaks observed in the 400 to 500 cm^{-1} region in the steamed crystals, whereas in the parent crystal the δ(Si–O) band at 470 cm^{-1} was dominant. In contrast, the bands in the 700–850 cm^{-1} (indicated by the orange area in Figure 2) were observed to increase in intensity in steamed crystals when compared to the parent crystal, with apparent loss of the ν(Si-O-Al) peak at 745 cm^{-1} upon steaming. These regions were chosen as the main areas of interest for further analysis.

The goodness-of-fit was determined with the chi-square test (χ^2). Table 2 summarizes the χ^2 results for the average Raman spectra of each zeolite ZSM-5 crystal under study. Further information regarding the goodness-of-fit calculation can be found in experimental section of the paper. The data collected from the first 4m starting from the P-ZSM-5 zeolite outer surface were not included in the chi-square calculation due to the high level of noise.

In the first part of our study, we have performed a *z*-stack analysis for which 5 μm × 5 μm areas were chosen in the middle of the Raman measurement layers. The spectra were averaged in these Raman maps measured for each zeolite

Table 2. Goodness-of-fit for the normalized and averaged Raman spectra of the zeolite ZSM-5 samples indicated by χ values. ($\chi^2 = 1$ ideal fit; $\chi^2 < 3$ convergence; $\chi^2 > 3$ minimum without convergence).

Sample	χ^2
P-ZSM-5	3.08
MT-ZSM-5	1.58
ST-ZSM-5	1.66

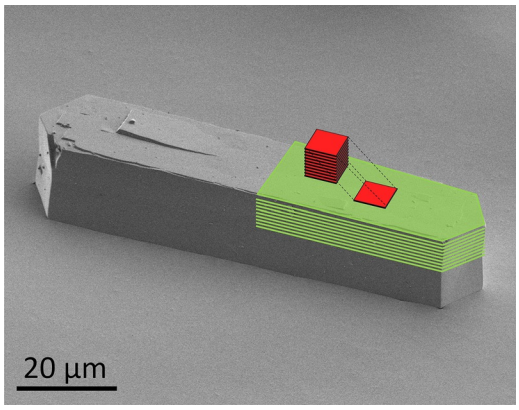

Figure 3. SEM image of a zeolite ZSM-5 crystal (100×20×20 μm). Green layers indicate the location of the Raman maps of the zeolite ZSM-5 crystal, whereas the analyzed volume for the *z*-stack analysis is shown by the indicated red cuboid (5×5×10 μm).

ZSM-5 crystal under study. A cuboid volume taken from each zeolite ZSM-5 crystal was evaluated. The location of the cuboid, with respect to the total measurement area is indicated in Figure 3. The first map was measured from the crystal surface, whereas the last map was measured from the mid-region (10 μm towards the crystal core starting from the outer surface).

The *z*-stack analysis of the normalized Raman spectra of a zeolite P-ZSM-5 crystal is shown in Figure 4a. In addition, the zoomed spectral regions of interest are shown in Figure 4b,c. The spectra measured from the first 4 layers (the first 4 μm starting from the zeolite outer surface) were too noisy, possibly due to a smaller amount of material within the laser focal area or due to lower scattering intensity of materials within the

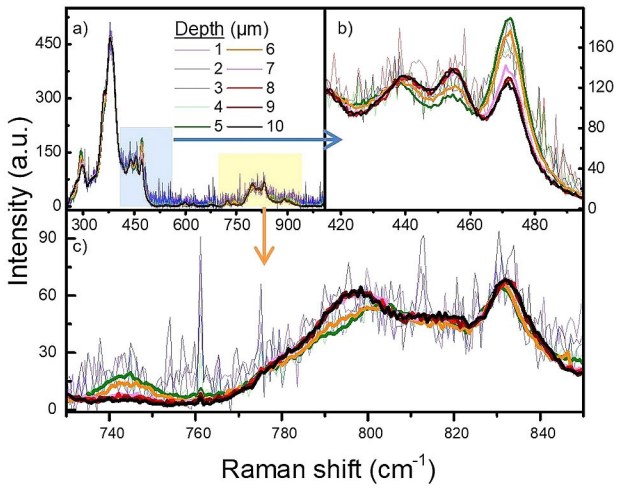

Figure 4. a) Normalized and averaged Raman spectra of each 2D Raman map of a large zeolite P-ZSM-5 crystal from the chosen area for *z*-stack analysis. Each map is numbered according to the depth they were measured from. The zoomed-in spectral region of the zeolite P-ZSM-5 crystal *z*-stack for the b) 400–500 cm^{-1} and c) 720–850 cm^{-1} spectral regions. The zoomed-in regions in panel (b) and (c) were highlighted in blue and orange, respectively. The spectral integration time was 7 s.

layers. Therefore, these spectra (spectra number 1–4) are shown in transparent colors so that they do not obscure the rest of the Raman spectra (spectra number 5–10).

The Raman band located at 438 cm^{-1}, ascribed to the stretching mode of the Si-O-Si bond, and the Raman band at 454 cm^{-1} that is the bending mode of the (O-Si-O(Al)) vibration, were observed to increase in intensity when moving towards the inner regions of the zeolite P-ZSM-5 crystal. The Raman band 470 cm^{-1} (ascribed to the bending mode of the (Si—O) vibration) showed the opposite behavior with respect to the measurement depth. In contrast, the spectral intensity of the Raman band located at 745 cm^{-1}, ascribed to the Si-O-Al bridge stretching mode, has been proposed in the literature to be a direct indicator of the Brønsted moiety (i.e., the amount of Brønsted acid sites).[24]

This Raman band decreased in intensity when moving towards the deeper regions of the zeolite crystal, as illustrated in Figure 4c. We have fitted the Voigt functions of this Raman band and calculated the area under each function, which was taken as a direct measure for the amount of Brønsted acid sites. Curve fitting details and parameters can be found in section S2 of the Supporting Information. We have used a least-squares polynomial fit to show the relationship between the amount of Brønsted sites (by taking the spectral intensity of the Raman band at 745 cm^{-1}) and the depth in the zeolite P-ZSM-5 crystal.

The results are summarized in Figure 5a. It is clear that the amount of Brønsted sites (and therefore the amount of framework Al species[57]) is characterized by an exponentially decaying trend when moving from the outer zeolite crystal surface towards the inner core of the zeolite crystal. The Raman band at 800 cm^{-1}, which was assigned to symmetric vibrations of Si-O-Si bonds showed an increase in deeper regions of the crystal. This trend possibly indicates the silicalite-rich inner zeolite core of the zeolite ZSM-5 crystal. The normalized average spectra comparison, shown in Figure 2, does not indicate clear intensity differences of the Raman active band present at 800 cm^{-1}. However, the Raman bands located at 814 and 832 cm^{-1} showed distinctive differences caused by steaming treatment. Therefore, we have investigated the trend of these two Raman bands at 814 and 832 cm^{-1} within a single P-ZSM-5 crystal, as shown in Figure 5b. None of these Raman bands showed a clear depth dependency.

We have applied the same *z*-stack analysis to a zeolite MT-ZSM-5 crystal and the corresponding spectra are shown in Figure 6. For the zeolite MT-ZSM-5 crystal measurement, the last 2D Raman map from the depth of 10 μm did not produce any meaningful results due to an instrumental error, and has therefore been excluded from our analysis. Unlike the Raman bands of the zeolite P-ZSM-5 crystal, the spectral intensity did not differ between the outer and inner regions of the crystal.

However, the Raman spectra themselves showed distinct differences when the parent and steamed zeolite crystals were compared. For instance, the relative spectral intensity differences for the Raman bands at 454 and 470 cm^{-1} were quite different for zeolite MT-ZSM-5 in comparison to zeolite P-ZSM-5. In addition, both Raman bands were clearly more intense for

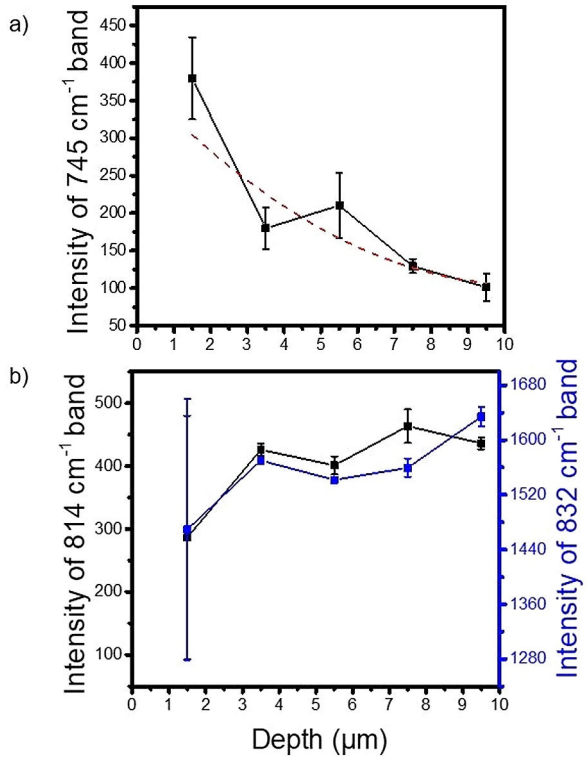

Figure 5. a) The relative amount of Brønsted acid sites (by determining the area under the fitted Voigt function of the 745 cm^{-1} Raman band from the averaged spectra shown in Figure 4) with respect to the zeolite P-ZSM-5 crystal depth. The red dashed curve shows the fitted polynomial function. b) The relative amount of Al–O bond (by determining the area under the fitted Voigt function of the 814 and 832 cm^{-1}) with respect to the zeolite P-ZSM-5 crystal depth.

P-ZSM-5 than for MT-ZSM-5. These differences can be explained by the effect of the steaming procedure on the structural integrity of the zeolite ZSM-5. The presence of water at elevated temperatures, in addition to thermal effects, causes the hydrolytic splitting of the Si-O-Al-bonds.[12] The Al species, leaving the zeolite framework, can migrate towards the formed mesopores[58] to create either framework species (Brønsted acid sites) or non-framework species.[59] This migration causes (partial) decomposition of the framework. The decomposed parts of the zeolite framework form silicic acid, which leads to healing of the Al vacancy.[60] The Raman bands at 454 and 470 cm^{-1}, therefore, could be used as a measure of the structural integrity of zeolite ZSM-5 crystals. On the other hand, no clear depth relation of the Raman band at 438 cm^{-1} was detected for the MT-ZSM-5 crystal compared to the P-ZSM-5 crystal. The Raman band located at 745 cm^{-1}, which indicates the presence of Brønsted acid sites, was less intense for all the measured layers of the zeolite MT-ZSM-5 crystal, as expected when compared to the zeolite P-ZSM-5 crystal. A least squares polynomial function was also fitted to the data to show the relationship between the amount of Brønsted acid sites and the measurement depth for the MT-ZSM-5 crystal. This is illustrated in Figure 7a. The decay trend of the Brønsted acidity concentration was observed to be more linearized. This means that the amount of Al near the top crystal surface decreased when compared to a parent zeolite ZSM-5 crystal. In contrast, the other Raman bands at 814 and 832 cm^{-1}, which are indicative for the Al distribution, had different trends with respect to the crystal depth for the zeolite MT-ZSM-5 crystal. The concentration of the Al species indicated by these bands were elevated in intensity below the near surface region (i.e., 2–5 μm depth), where the Al-enriched region is located.[44] This is illustrated in Figure 7b. The accumulation of migrated Al

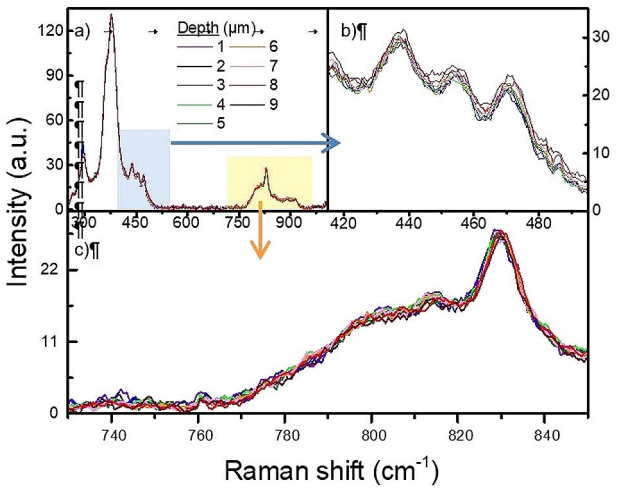

Figure 6. a) Normalized and averaged Raman spectra of each 2D Raman map of a large zeolite MT-ZSM-5 crystal from the chosen area for *z*-stack analysis. Each map is numbered according to the depth they were measured from. The zoomed-in spectral region of the zeolite MT-ZSM-5 crystal *z*-stack for the b) 400–500 cm^{-1} and c) 720–850 cm^{-1} spectral regions. The zoomed-in regions in panel (b) and (c) were highlighted in blue and orange, respectively. The spectral integration time was 7 s.

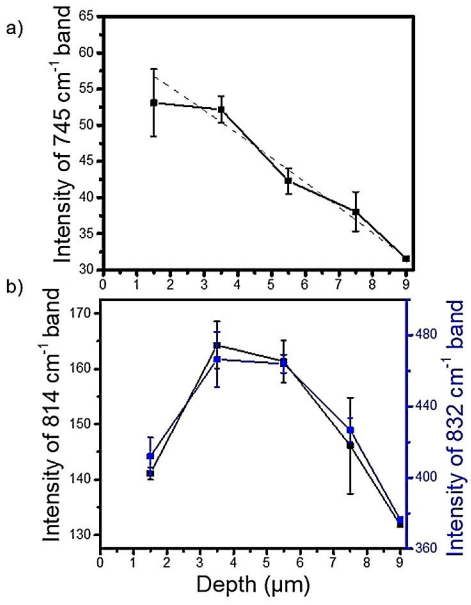

Figure 7. a) The relative amount of Brønsted acid sites (by determining the area under the fitted Voigt function of the 745 cm^{-1} Raman band from the averaged spectra shown in Figure 6) with respect to the zeolite MT-ZSM-5 crystal depth. The red dashed curve shows the fitted polynomial function. b) The relative amount of Al–O bond (by determining the area under the fitted Voigt function of the 814 and 832 cm^{-1}) with respect to the zeolite MT-ZSM-5 crystal depth.

species due to steaming is likely the cause for the elevated Al signal in this region. The band located at 800 cm^{-1} did not show any clear depth dependency for the zeolite MT-ZSM-5 crystal measurement. Finally, the *z*-stack analysis was performed on the zeolite ST-ZSM-5 crystal. The results are shown in Figure 8. The relative intensity of the Raman bands at 438,

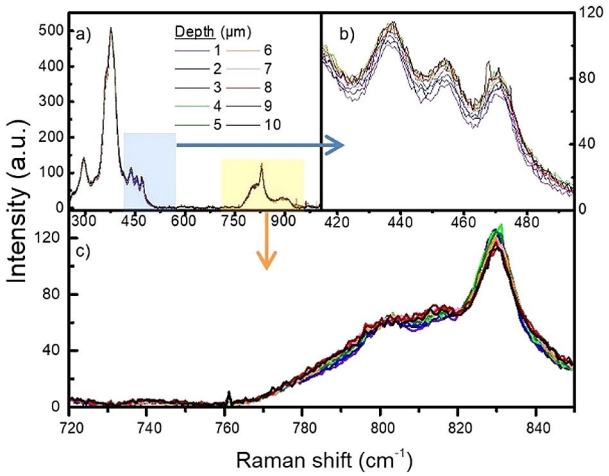

Figure 8. a) The relative amount of Brønsted acid sites (by determining the area under the fitted Voigt function of the 745 cm^{-1} Raman band) with respect to the zeolite ST-ZSM-5 crystal depth. The red dashed curve shows the fitted polynomial function. b) The relative amount of Al–O bond (by determining the area under the fitted Voigt function of the 814 and 832 cm^{-1}) with respect to the zeolite ST-ZSM-5 crystal depth.

454 and 470 cm^{-1}, which are assigned to ν(Si-O-Si), δ(O-Si-O(Al)), and δ(Si–O), respectively, indicated a similar distribution to the zeolite MT-ZSM-5 crystal. However, for the measurement of the P-ZSM-5 crystal, these bands were more depth-dependent and also had a different relative intensity distribution.

As we previously mentioned for the MT-ZSM-5 crystal measurement, the difference in the relative intensity of these Raman bands between the steamed and the parent zeolite ZSM-5 crystals may be related to the framework decomposition. Therefore, these bands might be an indicator for the structural integrity of the zeolite ZSM-5 framework. The distribution of Brønsted acid concentration was calculated through the comparison of the intensity profile of the spectral band at 745 cm^{-1}, as shown in Figure 9a. The decay trend indicated the Brønsted acidity dependency with depth was less pronounced.

Due to the severe steaming conditions, the migration of the Al species increased the Al concentration in the inner regions of the zeolite crystal. This migration can also be followed with the intensity profiles of the Raman bands at 814 and at 832 cm^{-1}, as shown in Figure 9b. Their trends were similar to the zeolite MT-ZSM-5 crystal. An increase of the intensities of these two Raman bands indicates a spatial enrichment of specific Al–O vibrations, possibly due to the increase of split Al species from the outer regions of the framework. As explained before, both of these Raman bands were previously assigned to vibrations of Al species. Similar to the MT-ZSM-5 measure-

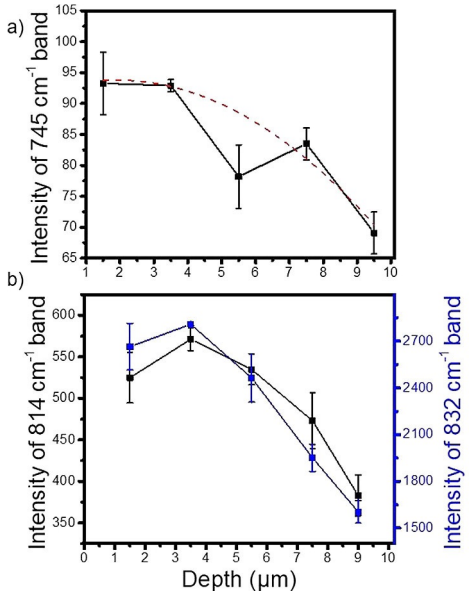

Figure 9. a) The relative amount of Brønsted acid sites (by determining the area under the fitted Voigt function of the 745 cm^{-1} Raman band from the averaged spectra shown in Figure 8) with respect to the zeolite ST-ZSM-5 crystal depth. The red dashed curve shows the fitted polynomial function. b) The relative amount of Al–O bond (by determining the area under the fitted Voigt function of the 814 and 832 cm^{-1}) with respect to the zeolite ST-ZSM-5 crystal depth.

ment, no clear depth dependency for the band located at 800 cm^{-1} was observed. This indicates that the Si-O-Si network, reflected in changes to the 800 cm^{-1} band, does not change significantly with depth. Our experiments showed a similar intensity trend of the Raman bands 814 and 832 cm^{-1}, but a different trend of the band 745 cm^{-1}. The band at 745 cm^{-1} has been related to framework Al species, thus Brønsted acid moieties, suggesting that these species decrease in number with depth in the ST-ZSM-5 crystal. Previous work has also attributed the 814 and 832 cm^{-1} bands to Al species. However, their contrasting change in intensity with depth, compared to the framework Al band at 745 cm^{-1}, implies that they are not related to framework Al, therefore, we have assigned them to extra-framework Al species. The increase of both these bands indicates that the extra-framework Al species in the Al rich region (that is inherent to these large zeolite ZSM-5 crystals) is possibly due to the steric hindrance created by framework decomposition.

The formation of non-framework Al due to steam treatment was shown previously by our group to occur mainly in the Al-rich domains, rather than Al-poor regions, by 2D μXRD measurements on single zeolite ZSM-5 crystals.[12]

Z-stack analysis showed layer by layer Brønsted acid distribution, crystal integrity variation and the distribution of extra-framework Al species with respect to crystal pre-treatment. However, all these variations were observed in pre-defined regions and thus only portray changes related to the *z*-direction rather than the whole analysis volume. In order to obtain the distribution of structural and chemical variations in all the measurement volume, principal component analysis (PCA) and subsequent clustering analysis (CA) were performed. In this

case, instead of a specific location on the zeolite ZSM-5 crystals we analyzed the complete spectra from each point obtained within every mapped area (indicated in green in Figure 3).

In order to simplify the 3D dataset that contains thousands of individual Raman spectra, each map was clustered into six regions that have distinct and most similar spectral features. The PCA and clustering analysis result for each crystal is shown in Figure 10a–c. The averaged Raman spectra of the clusters are shown in Figure 10d–f. Clustering analysis distinguished the background of the Raman measurements from the real fingerprint spectra. Cluster number 2 (the blue cluster) was identified as the background for all the zeolites measured. We observed that the background cluster for each zeolite crystal slightly shifts in the maps taken from the deeper regions of the crystal. This could be caused by increased scattering effects in the Raman micro-spectroscopy measurements from the deeper locations, a potential shift of the measurements when looked at as separate 2D layers. Therefore, cluster number 2 from each map was not considered in further analysis.

Clustering analysis showed that the overall heterogeneity increased due to steaming specifically near the crystal surface regions for both steamed zeolite ZSM-5 crystals. The zoomed-in Raman spectra of the regions of interest are shown in Figure 11. The relative intensities of the Raman bands between

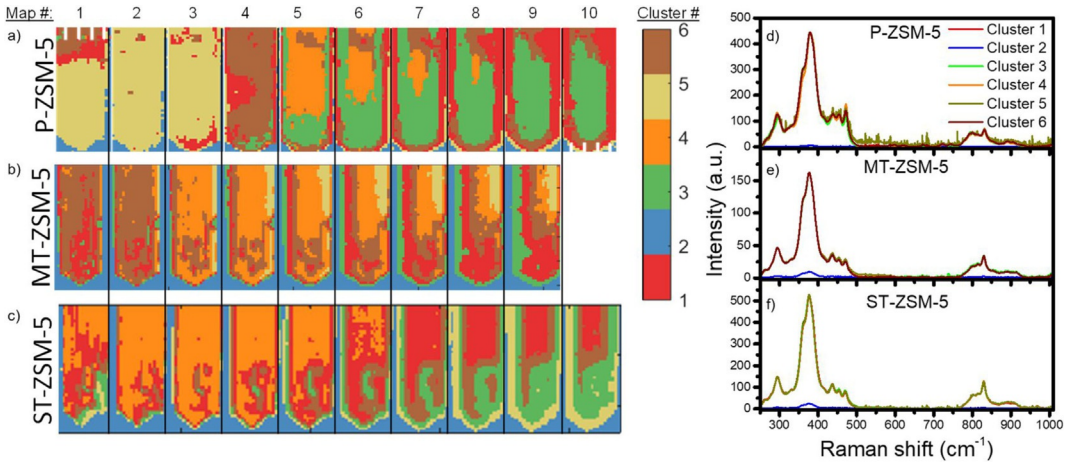

Figure 10. Clustering results of each individual 2D Raman map of a zeolite a) P-ZSM-5, b) MT-ZSM-5 and c) ST-ZSM-5 crystal. Images are numbered from the zeolite surface towards the zeolite core. On the right hand side, numbering of the color-coded clusters are given. The normalized, averaged Raman spectra of the respective clusters of the zeolite d) P-ZSM-5 e) MT-ZSM-5 f) ST-ZSM-5 crystal. 3D Raman map. The spectral integration time was 7 s.

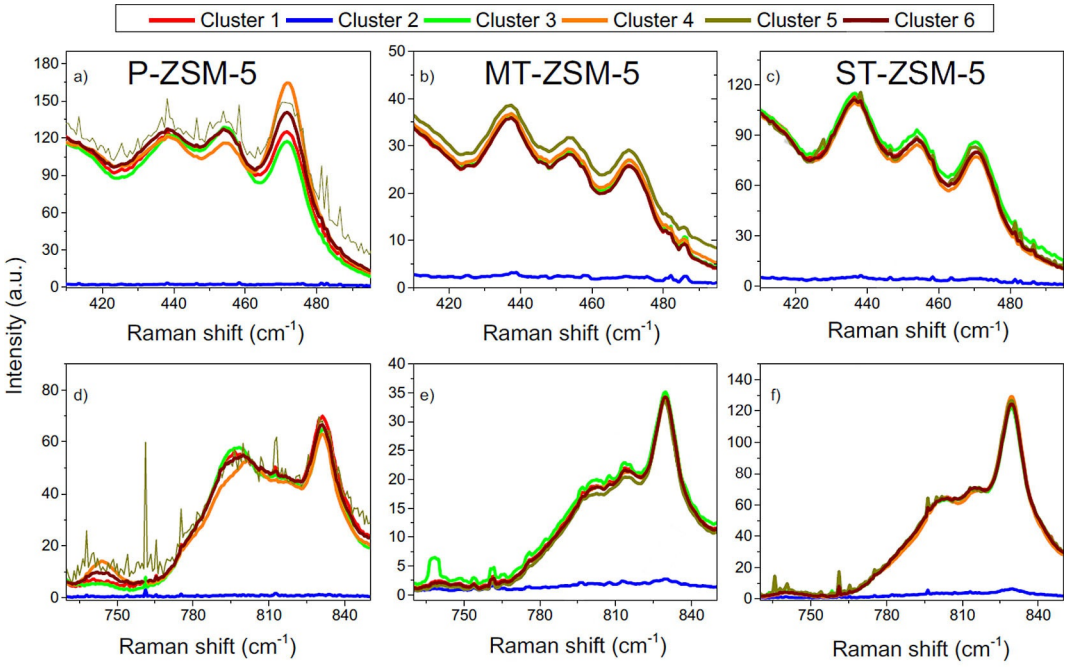

Figure 11. The zoomed-in normalized, mean cluster Raman spectra of the zeolite ZSM-5 crystal analyzed. 410–490 cm^{-1} spectral region of the zeolite a) P-ZSM-5, b) MT-ZSM-5 and c) ST-ZSM-5 crystal and 720–850 cm^{-1} region of the zeolite d) P-ZSM-5, e) MT-ZSM-5 and f) ST-ZSM-5 crystal.

400 and 500 cm^{-1} were lower for the two steamed zeolite ZSM-5 crystals than for the parent zeolite ZSM-5 crystal. As these Raman bands can be related to zeolite structural integrity, the influence of the hydrothermal treatment can also be observed in the PCA and CA. PCA and CA also showed an increase of the Raman bands in the 800 cm^{-1} region that are indicative for the presence of extra-framework Al species for the steamed zeolite ZSM-5 crystals. Cluster number 3 for the zeolite MT-ZSM-5 crystal and cluster number 5 for the zeolite ST-ZSM-5 crystal had relatively higher intensity for both of these Raman bands. Both these mentioned clusters are located in the crystal rims. Therefore, PCA and CA indicate that extra-framework Al is more abundant at the near edge regions in the steamed zeolite ZSM-5 crystals.

Conclusions

Large zeolite ZSM-5 crystals were mapped with 3D Raman spectroscopy to identify the chemical structure of the zeolite framework. Furthermore, the structural and chemical changes occurring during a steam treatment (at 500 and 700 °C) were investigated. The Raman active vibrational modes of zeolite ZSM-5 that are related to Brønsted acid sites, defect sites, as well as structural integrity, were identified. Our experimental findings can serve as inspiration for theoreticians to further refine the assignments of vibrational modes of zeolite-based materials.

Typical Raman bands, which are linked to zeolite structure integrity, are located at 454 and 470 cm^{-1}. The intensity of these two Raman bands decreases with increasing steaming severity. In addition, another structure-related Raman band was identified at 438 cm^{-1}, which was found to be an indicator for the replacement of Al species by Si species. The band located at 800 cm^{-1} was also related to the structural integrity of the zeolite framework. Extra-framework Al species were characterized by Raman bands at 814 and 832 cm^{-1}. The amount of Brønsted acid sites (directly associated with framework Al distribution), which was correlated with a Raman band at 745 cm^{-1}, was observed to change due to steaming.

3D Raman spectroscopy confirmed the presence of a gradually decreasing Al distribution from outer crystal surface towards the crystal core in the large zeolite ZSM-5 crystals. The increasing heterogeneity upon steaming the zeolite ZSM-5 crystals was observed to be more prominent in the near-surface regions than in the crystal center. Defect sites are also formed in this steaming process, mainly in the near-surface regions of the zeolite ZSM-5 crystals. Further heterogeneities induced by steaming were followed by assessing the migration of framework Al species as well as the formation of extra-framework Al species. Upon steaming, the Al sites that are enriched in the near surface region of the zeolite crystal partially move towards the center of the zeolite crystal, meanwhile, the remaining framework sites are filled with Si atoms. The relocated extra-framework Al species also accumulate inside the Al-rich region due to steric hindrance, thereby forming partially extra-framework Al species.

Experimental Section

Large zeolite ZSM-5 crystals with a size of 100×20×20 μm (bulk Si/Al: 17) were provided by ExxonMobil (Machelen, Belgium) in their Na^+ form. The starting chemicals for the synthesis of these zeolite ZSM-5 crystals were: Ludox AS40 (40 wt.% in H_2O, Sigma-Aldrich), tetrapropylammonium bromide (TPABr, Fluka, ≥98%), $Al_2(SO_4)_3{\cdot}18\,H_2O$ (Baker, 98%), and NH_4OH (VWR, 29%). The molar composition of the synthesis gel was $6.65\,(NH_4)_2O/0.67\,TPA_2O/0.025\,Al_2O_3/10\,SiO_2/121\,H_2O$. Their synthesis and details on these materials have been reported in detail elsewhere[11,49–54] Both template removal and steaming were performed in the same manner as previous studies conducted in our group.[11,54] The as-synthesized samples were first calcined at 500 °C with ramp rate of 1 °C min^{-1} for 12 h in air to remove the template in a flow oven. Subsequently, a triple ion exchange with a 10 wt.% ammonium nitrate (Acros Organics, >99%) solution was performed at 60 °C. After the repetition of the calcination step, the zeolite P-ZSM-5 crystals were obtained. Hydrothermal treatment (steaming) was performed in a quartz tubular oven (a Thermoline 79300 instrument) that was preheated to 120 °C. The zeolite P-ZSM-5 crystals were placed in the oven and water vapor (at 100 °C) was introduced into the tubular oven for 5 h at 500 °C to obtain mildly treated (MT-ZSM-5) and at 700 °C to obtain severely treated (ST-ZSM-5) zeolites. N_2 with a flow rate of 180 mL min^{-1} was used as the carrier gas. A follow-up calcination was performed in a static oven at 500 °C for 8 h for both of the steamed samples.

Three-dimensional (3D) Raman spectroscopy measurements were recorded using a high-resolution WITec alpha 300R Raman microscope using a 532 nm Nd:YAG laser with 14 mW power. The Raman spectra were measured in the range of 250–1000 cm^{-1}, that is, encompassing the region with the highest intensity bands for the zeolite structure. The spatial resolution of the Raman microscopy measurements in the *xy* directions was calculated to be 0.4 μm. The confocality of the Raman spectrometer results in an estimated 1 μm depth resolution with the 100x objective lens (N.A. = 0.9) used in the analysis. These calculations were done according to reference.[17] The 3D Raman spectroscopy datasets for each zeolite ZSM-5 crystal under study consists of ten two dimensional (2D) maps measured in 50×20 μm areas. An argon-mercury light source was used to calibrate the instrument. After scattering from the sample, the Raman light was collected in a 180° backscattering geometry and diffracted using an 1800 grooves mm^{-1} grating before reaching the Charge Coupled Device (CCD) detector. This instrument configuration produces a band resolution of 2 cm^{-1} in the spectral region of interest, as measured using the full width at half maximum of bands generated by an in-built calibration light source. Tilt of the sample was removed using an automated topography correction. This correction is based on *z*-stage position that was logged for the focal point observed in the optical image of the crystal surface at 25 evenly distributed points across the mapping area. This correction was applied to each of the maps independently so that the maps do not include the sample tilt in the *xy* plane.

For each zeolite crystal 2D Raman maps were acquired beginning at the crystal surface before the stage was lowered by 1 μm and a second 2D map was acquired. The confocality capability of the Raman spectrometer means that the entire volume can be analyzed at 1 μm depth resolution by focusing at increasingly deeper points within the crystal. In total half of the crystal depth (10 μm) could be probed. This corresponded to a quarter of an entire zeolite crystal as they were typically 100 μm long, thus twice the length of the mapped area. The collected 3D datasets were ana-

lyzed using two different methods. A *z*-stack analysis was performed where we aimed to elucidate the modifications caused by steaming at 500 and at 700 °C with respect to the measurement depth. As the middle region of these large zeolite ZSM-5 crystals showed very similar characteristics in a single 2D layer, we have averaged the spectra from a 5×5 μm area in the mid-region of each 2D Raman map (Figure 3). This analysis was performed for each measurement. Samples are sprinkled on an indium stub. The surface of the stub was subsequently flattened using a press tool. In this way, the samples were fixed on the stubs for the duration of the mapping measurements. Samples were measured under ambient conditions.

The second analysis on the 3D Raman maps of the zeolite ZSM-5 crystals was performed using principal component analysis (PCA). PCA represents the dataset without using any a priori knowledge about the data characteristics,[61–63] and was used to reduce the hyper-dimensional 3D Raman data set to *N*, that is 1600 for this study, components by choosing the first 4 principal components covering a cumulative variance explained (CVE) of 97%. In this way, no significant information was lost but the noise could be reduced. Subsequent *k*-means clustering was used to cluster all data points (representing all voxels of the data set) in the space spanned by these *N* first PCs with respect to their Euclidian distances from the cluster centers using the centroid linkage method.[64,65] With this approach, the voxels with most similar Raman spectra (i.e., data points close to each other in PC space) were pooled. PCA and clustering analysis was performed using an in-house-developed software package (XANES-Wizard).[66]

Raman spectra obtained from the *z*-stack analysis, and PCA and clustering, were fitted with the Fityk software using Voigt functions. Voigt functions were chosen for fitting as they have characteristics of both Gaussian and Lorentzian profiles.[67] Curve fitting for the determination of spectral parameters was performed with the software program Origin 9.0. The goodness-of-fit was indicated by the χ^2 value, which indicates the agreement between the calculated fit curve and the observed spectrum. Values between 1 and 3 imply that the curve fit converges towards the observed spectrum; values larger than 3 indicate that the iteration has reached a minimum, but does not converge.[68]

Acknowledgements

Dr. Machteld Martens (ExxonMobil, Belgium) is acknowledged for providing the large zeolite ZSM-5 crystals. B.M.W. acknowledges The Netherlands Organization for Scientific Research (NWO) for a Gravitation program (Netherlands Center for Multiscale Catalytic Energy Conversion, MCEC) and a European Research Council (ERC) Advanced Grant (grant no. 321140).

Conflict of interest

The authors declare no conflict of interest.

Keywords: aluminum zoning · Raman spectroscopy · steaming · zeolite

[1] M. E. Davis, *Ind. Eng. Chem. Res.* **1991**, *30*, 1675 – 1683.
[2] C. B. Khouw, M. E. Davis in *Selectivity in Catalysis. ACS Symposium Series, Vol. 517* (Eds.: M. E. Davis, S. L. Suib), ACS Publications, Washington, D.C., **1993**, pp. 206 – 221.
[3] G. Busca, *Chem. Rev.* **2007**, *107*, 5366 – 5410.
[4] A. Samoson, E. Lippmaa, G. Engelhardt, U. Lohse, H. G. Jerschkewitz, *Chem. Phys. Lett.* **1987**, *134*, 589 – 592.
[5] P. Sazama, J. Dědeček, V. Gábová, B. Wichterlová, G. Spoto, S. Bordiga, *J. Catal.* **2008**, *254*, 180 – 189.
[6] I. M. Dahl, S. Kolboe, *Catal. Lett.* **1993**, *20*, 329 – 336.
[7] M. Stöcker, *Microporous Mesoporous Mater.* **1999**, *29*, 3 – 48.
[8] D. Lesthaeghe, A. Horré, M. Waroquier, G. B. Marin, V. Van Speybroeck, *Chem. Eur. J.* **2009**, *15*, 10803 – 10808.
[9] M. Bjørgen, F. Joensen, K. P. Lillerud, U. Olsbye, S. Svelle, *Catal. Today* **2009**, *142*, 90 – 97.
[10] H. van Bekkum, E. M. Flanigen, P. A. H. Jacobs, J. C. Jansen, *Introduction to Zeolite Science and Practice*, Elsevier, Amsterdam, **2001**.
[11] L. R. Aramburo, L. Karwacki, P. Cubillas, S. Asahina, D. A. M. de Winter, M. R. Drury, I. L. C. Buurmans, E. Stavitski, D. Mores, M. Daturi, P. Bazin, P. Dumas, F. Thibault-Starzyk, J. A. Poost, M. W. Anderson, O. Terasaki, B. M. Weckhuysen, *Chem. Eur. J.* **2011**, *17*, 13773 – 13781.
[12] Z. Ristanović, J. P. Hofmann, M. I. Richard, T. Jiang, G. A. Chahine, T. U. Schülli, F. Meirer, B. M. Weckhuysen, *Angew. Chem. Int. Ed.* **2016**, *55*, 7496 – 7500; *Angew. Chem.* **2016**, *128*, 7622 – 7626.
[13] L. Karwacki, D. A. M. De Winter, L. R. Aramburo, M. N. Lebbink, J. A. Post, M. R. Drury, B. M. Weckhuysen, *Angew. Chem. Int. Ed.* **2011**, *50*, 1294 – 1298; *Angew. Chem.* **2011**, *123*, 1330 – 1334.
[14] L. R. Aramburo, S. Wirick, P. S. Miedema, I. L. C. Buurmans, F. M. F. de Groot, B. M. Weckhuysen, *Phys. Chem. Chem. Phys.* **2012**, *14*, 6967 – 6973.
[15] P. P. Knops-Gerrits, D. E. de Vos, E. J. P. Feijen, P. A. Jacobs, *Microporous Mater.* **1997**, *8*, 3 – 17.
[16] a) E. Stavitski, B. M. Weckhuysen, *Chem. Soc. Rev.* **2010**, *39*, 4615 – 4625; b) S. Bordiga, C. Lamberti, F. Bonino, A. Travert, F. Thibault-Starzyk, *Chem. Soc. Rev.* **2015**, *44*, 7262 – 7341.
[17] R. H. Webb, *Rep. Prog. Phys.* **1996**, *59*, 427 – 471.
[18] Y. Yu, G. Xiong, C. Li, F. S. Xiao, *Microporous Mesoporous Mater.* **2001**, *46*, 23 – 34.
[19] C. Li, P. C. Stair, *Catal. Today* **1997**, *33*, 353 – 360.
[20] S. Jin, Z. Feng, F. Fan, C. Li, *Catal. Lett.* **2015**, *145*, 468 – 481.
[21] P. K. Dutta, D. C. Shieh, M. Puri, *J. Phys. Chem.* **1987**, *91*, 2332 – 2336.
[22] Y. T. Chua, P. C. Stair, *J. Catal.* **2003**, *213*, 39 – 46.
[23] M. Signorile, F. Bonino, A. Damin, S. Bordiga, *J. Phys. Chem. C* **2015**, *119*, 11694 – 11698.
[24] M. Signorile, F. Bonino, A. Damin, S. Bordiga, *J. Phys. Chem. C* **2016**, *120*, 18088 – 18092.
[25] E. M. Flanigen, H. Khatami, H. A. Szymanski in *Advances in Chemistry, Vol. 101* (Eds.: E. M. Flanigen, L. B. Sand), ACS Publications, Washington, D.C., **1974**, pp. 201 – 229.
[26] W. B. White, R. Roy, *Am. Mineral.* **1964**, *49*, 1670 – 1687.
[27] P. K. Dutta, J. Twu, *J. Phys. Chem.* **1991**, *95*, 2498 – 2501.
[28] P. K. Dutta, B. Del Barco, *J. Phys. Chem.* **1988**, *92*, 354 – 357.
[29] P. K. Dutta, M. Puri, *J. Phys. Chem.* **1987**, *91*, 4329 – 4333.
[30] "Vibrational Spectroscopy": H. G. Karge, E. Geidel in *Molecular Sieves, Vol. 4*, Springer, Berlin, **2004**, pp. 1 – 200.
[31] P. K. Dutta, K. M. Rao, J. Y. Park, *J. Phys. Chem.* **1991**, *95*, 6654 – 6656.
[32] S. Auerbach, K. Carrado, P. Dutta, *Handbook of Zeolite Science and Technology*, CRC Press, New York, **2003**.
[33] C. S. Blackwell, *J. Phys. Chem.* **1979**, *83*, 3251 – 3257.
[34] S. Bohra, D. Kundu, M. K. Naskar, *Ceram. Int.* **2014**, *40*, 1229 – 1234.
[35] K. K. Gorshunova, O. S. Travkina, M. L. Pavlov, B. I. Kutepov, R. Z. Kuvatova, N. A. Amineva, *Russ. J. Appl. Chem.* **2013**, *86*, 1805 – 1810.
[36] E. Geidel, H. Böhlig, C. Peuker, W. Pilz, *Stud. Surf. Sci. Catal.* **1991**, *65*, 511 – 519.
[37] R. Szostak, *Molecular Sieves Principles of Synthesis and Identification*, Springer, New York, **1989**.
[38] M. Bärtsch, P. Bornhauser, G. Calzaferri, R. Imhof, *Stud. Surf. Sci. Catal.* **1994**, *84*, 2089 – 2098.
[39] P. Bornhauser, G. Calzaferri, *J. Phys. Chem.* **1996**, *100*, 2035 – 2044.
[40] S. R. Stojkovic, B. Adnadjevic, *Zeolites* **1988**, *8*, 523 – 525.
[41] S. P. Zhdanov, T. I. Titova, L. S. Kosheleva, W. Lutz, *Pure Appl. Chem.* **1989**, *61*, 1977 – 1980.
[42] G. Wengui, L. Juan, L. Hongyuan, Y. Muliang, H. Jiehan, *IR Study of Framework Vibrations and Surface Properties of High Silica Zeolites*, Elsevier, Amsterdam, **1985**.

[43] R. Belaabed, S. Elabed, A. Addaou, A. Laajab, M. A. Rodríguez, A. Lahsini, *Bol. Soc. Esp. Ceram. Vidrio* **2016**, *55*, 152 – 158.
[44] R. von Ballmoos, W. M. Meier, *Nature* **1981**, *289*, 782 – 783.
[45] E. G. Derouane, S. Determmerie, Z. Gabelica, N. Blom, *Appl. Catal.* **1981**, *1*, 201 – 224.
[46] R. Althoff, B. Schulz-Dobrick, F. Schüth, K. Unger, *Microporous Mater.* **1993**, *1*, 207 – 218.
[47] J. B. Nagy, P. Bodart, H. Collette, J. El Hage-Al Asswad, Z. Gabelica, R. Aiello, A. Nastro, C. Pellegrino, *Zeolites* **1988**, *8*, 209 – 220.
[48] G. Debras, A. Gourgue, J. B. Nagy, G. De Clippeleir, *Zeolites* **1985**, *5*, 369 – 376.
[49] L. Karwacki, M. H. F. Kox, D. A. M. de Winter, M. R. Drury, J. D. Meeldijk, E. Stavitski, W. Schmidt, M. Mertens, P. Cubillas, N. John, A. Chan, N. Kahn, S. R. Bare, M. Anderson, J. Kornatowski, B. M. Weckhuysen, *Nat. Mater.* **2009**, *8*, 959 – 968.
[50] E. Stavitski, M. R. Drury, D. A. M. de Winter, M. H. F. Kox, B. M. Weckhuysen, *Angew. Chem. Int. Ed.* **2008**, *47*, 5637 – 5640; *Angew. Chem.* **2008**, *120*, 5719 – 5722.
[51] E. Stavitski, M. H. F. Kox, I. Swart, F. M. F. de Groot, B. M. Weckhuysen, *Angew. Chem. Int. Ed.* **2008**, *47*, 3543 – 3547; *Angew. Chem.* **2008**, *120*, 3599 – 3603.
[52] L. Karwacki, E. Stavitski, M. H. F. Kox, J. Kornatowski, B. M. Weckhuysen, *Angew. Chem. Int. Ed.* **2007**, *46*, 7228; *Angew. Chem.* **2007**, *119*, 7366.
[53] M. H. F. Kox, E. Stavitski, B. M. Weckhuysen, *Angew. Chem. Int. Ed.* **2007**, *46*, 3652 – 3655; *Angew. Chem.* **2007**, *119*, 3726 – 3729.
[54] Z. Ristanović, J. P. Hofmann, G. De Cremer, A. V. Kubarev, M. Rohnke, F. Meirer, J. Hofkens, M. B. J. Roeffaers, B. M. Weckhuysen, *J. Am. Chem. Soc.* **2015**, *137*, 6559 – 6568.
[55] P. Larkin, *IR and Raman Spectroscopy: Principles and Spectral Interpretation*, Elsevier, Oxford, **2011**.
[56] A. Zoubir, *Raman Imaging*, Springer, Berlin, **2012**.
[57] Z. Ristanović, J. P. Hofmann, U. Deka, T. U. Schülli, M. Rohnke, A. M. Beale, B. M. Weckhuysen, *Angew. Chem. Int. Ed.* **2013**, *52*, 13382 – 13386; *Angew. Chem.* **2013**, *125*, 13624 – 13628.
[58] C. Choifeng, J. B. Hall, B. J. Huggins, R. A. Beyerlein, *J. Catal.* **1993**, *140*, 395 – 405.
[59] D. Coster, A. L. Blumenfeld, J. J. Fripiat, *J. Phys. Chem.* **1994**, *98*, 6201 – 6211.
[60] N. Salman, C. H. Rüscher, J. C. Buhl, W. Lutz, H. Toufar, M. Stöcker, *Microporous Mesoporous Mater.* **2006**, *90*, 339 – 346.
[61] I. T. Jolliffe, *Principal Component Analysis*, Springer, New York, **2002**.
[62] R. Bro, A. K. Smilde, *Anal. Methods* **2014**, *6*, 2812 – 2831.
[63] R. A. Johnson, D. W. Wichern, *Applied Multivariate Statistical Analysis*, Prentice-Hall, Upper Saddle River, **2008**.
[64] J. A. Hartigan, M. A. Wong, *Appl. Stat.* **1979**, *28*, 100 – 108.
[65] S. L. Bieber, D. V. Smith, *Chem. Senses* **1986**, *11*, 19 – 47.
[66] Y. Liu, F. Meirer, P. A. Williams, J. Wang, J. C. Andrews, P. Pianetta, *J. Synchrotron Radiat.* **2012**, *19*, 281 – 287.
[67] T. Váczi, *Appl. Spectrosc.* **2014**, *68*, 1274 – 1278.
[68] A. Sadezky, H. Muckenhuber, H. Grothe, R. Niessner, U. Poschl, *Carbon* **2005**, *43*, 1731 – 1742.

Manuscript received: November 13, 2018
Revised manuscript received: February 25, 2019
Accepted manuscript online: March 3, 2019
Version of record online: May 2, 2019

